TITLE: A GALLIUM-68-LABELED PEPTIDE RADIOTRACER FOR CD38-TARGETED IMAGING IN MULTIPLE MYELOMA WITH PET.

Ajay Kumar Sharma[1±], Kuldeep Gupta[1±], Akhilesh Mishra[1,2], Gabriela Lofland[1], Ian Marsh[1], Dhiraj Kumar[1], Gabriel Ghiaur[3], Philip Imus[3], Robert F. Hobbs[1], Christian B. Gocke[3], and Sridhar Nimmagadda[1, 3, 4, 5, *]

Author affiliations:
[1]The Russell H. Morgan Department of Radiology and Radiological Science
[2]Chemical & Biomolecular Engineering, Whiting School of Engineering
[3]The Sidney Kimmel Comprehensive Cancer Center and the Bloomberg–Kimmel Institute for Cancer Immunotherapy
[4]Department of Pharmacology and Molecular Sciences
[5]Division of Clinical Pharmacology, Department of Medicine,
Johns Hopkins University School of Medicine,
Baltimore, MD, 21287, USA.
[±]Co-first authors

*Correspondence to: Sridhar Nimmagadda, Ph.D.
Johns Hopkins Medical Institutions
1550 Orleans Street, CRB II, #491
Baltimore, MD 21287
Phone: 410-502-6244
Fax: 410-614-3147
Email: snimmag1@jhmi.edu

Running title: New Radiotracer for CD38-Targeted Imaging in Multiple Myeloma

Key words: CD38, PET, Daratumumab, Dsatuximab, Minimal residual disease

Funding: This study was funded by NIH 1R01CA236616 (SN) and the Ga-68 generator was supported by NIH R01CA269235. Core resources (histology and imaging) were supported by NIH P30CA006973.

STATEMENT OF TRANSLATIONAL RELEVANCE

Multiple myeloma is a challenging bone marrow plasma cell disease that is associated with heterogenous responses and universal recurrence. While minimal residual disease monitoring by blood and invasive bone marrow samples have improved prognostication of disease recurrence, molecularly targeted non-invasive imaging options remain limited. Additionally, there is an unmet need for functional imaging agents to monitor the effects of new therapeutics targeting CD38 protein, which is highly expressed on MM cells. To address this gap, we report the development of a high affinity first-in-class gallium-68 labeled peptide radiotracer for CD38, [^{68}Ga]Ga-AJ206. [^{68}Ga]Ga-AJ206 provides high-contrast images by PET within the standard clinical workflow of 60 minutes. Furthermore, we have demonstrated the potential of [^{68}Ga]Ga-AJ206 PET to measure varying levels of CD38 expression. Further development of this new radiotracer may complement existing technologies and improve prognostication and monitoring of therapy response in MM patients.

ABSTRACT

Purpose. We aimed to develop a novel molecular imaging agent to monitor Multiple Myeloma (MM) using CD38, a target that has shown uniform expression in MM. However, only a few molecularly targeted imaging agents are available to take advantage of this high expression and the sensitivity of positron emission tomography (PET), and none of them fit into the standard clinical workflow. To address this, we developed and evaluated a first-in-class peptide-based radiotracer, [^{68}Ga]Ga-AJ206, to non-invasively quantify CD38 levels in MM.

Experimental design. To quantify CD38 levels non-invasively, we synthesized a peptide-based high-affinity binder, tested its affinity by surface plasmon resonance, and evaluated a gallium-68–labeled analog for in vitro specificity. We also performed in vivo distribution, pharmacokinetics, and CD38 specificity evaluations in MM preclinical models, and cross-validated imaging data with flow cytometry and immunohistochemistry-based analysis of CD38 expression.

Results. [^{68}Ga]Ga-AJ206 demonstrated CD38 binding specificity with a dissociation constant (K_D) of 19.1±0.99 nM and in vitro binding dependent on CD38 expression. PET imaging with [^{68}Ga]Ga-AJ206 showed high contrast within 60 min and suitable radiation dose estimates for clinical use. Additionally, [^{68}Ga]Ga-AJ206 detected CD38 expression in xenograft and disseminated disease models in a manner consistent with immunohistochemistry-based detection.

Conclusions. [^{68}Ga]Ga-AJ206 exhibited the salient features required for clinical translation, providing CD38-specific high contrast images and detecting varying levels of CD38 expression in bone disease and soft tissue metastases.

INTRODUCTION.

Multiple myeloma (MM) is a type of blood cancer that affects plasma cells in the bone marrow(1). It is characterized by wide variability in response to therapy and survival due to its biological heterogeneity(1). Standard-of-care options for MM include combinations of drugs with different mechanisms of action, such as proteasome inhibitors (PIs), immunomodulatory drugs (IMIDs), histone deacetylase inhibitors (iHDACs), monoclonal antibodies targeting several antigens (mAbs), and high-dose chemotherapy rescued by autologous stem cell transplantation (ASCT). Continuous therapy with a combination of those agents has been associated with the best outcomes(2). However, there are efforts underway to tailor or taper treatment in patients who have little or no detectable minimal residual disease (MRD) to reduce toxicity(3). As a result, the accurate detection of small amounts of disease will become increasingly important for this growing patient population.

Current methods to quantify the burden of MM in patients includes bone marrow biopsies, serum testing of monoclonal paraprotein, and cross-sectional imaging(4,5). Among the latter, positron emission tomography combined with computed tomography (PET-CT) is the best equipped to determine response to treatment and provide prognostic information(6). Most patients with MM who do not meet CRAB criteria (hypercalcemia, renal dysfunction, anemia, and lytic bone lesions) are also monitored with PET-CT(4). However, the specificity of the imaging agent used in PET-CT, [^{18}F]FDG, is limited at 78%(7,8). The development of molecularly targeted imaging agents that can enhance the specificity and sensitivity of MM detection while utilizing the functional sensitivity of PET-CT is necessary.

To improve specificity and sensitivity to detect MM, several groups have developed molecularly targeted imaging agents leveraging the high expression of cluster of differentiation protein 38 (CD38) on MM cells(9-18). CD38 is a type II transmembrane glycoprotein with an ectozyme activity and a receptor(19,20). Under physiological conditions, CD38 is expressed at low levels on myeloid and lymphoid cells(19,20). In contrast, CD38 protein is expressed uniformly and with high density in MM, making it a promising target for non-invasive detection of MM disease burden. Taking advantage of high CD38 expression, several CD38-targeting therapies including anti-CD38 antibodies have been developed or in different phases of clinical development(21). Additionally, radiolabeled conjugates of anti-CD38 antibodies have been shown to detect MM in preclinical models and patients with superior specificity and sensitivity compared to [^{18}F]FDG-PET(9,15). However, the use of low molecular weight agents for CD38 targeting has not been reported for MM. In this regard, peptides, which have high specificity, fast clearance, and are easily synthesized, are increasingly being used as cancer-targeting tools. Peptide-radiotracers can enhance contrast and lesion detection due to their faster clearance times compared to antibodies (hours *vs*. days). In this study, we took advantage of these characteristics to develop a novel peptide-based low molecular weight agent for CD38 that can detect disease in the whole body within a few hours.

Here, we report the development and evaluation of a new gallium-68 labeled peptide-based radiotracer for CD38 targeting in multiple myeloma (MM). The radiotracer, [^{68}Ga]Ga-AJ206, showed substantially improved pharmacokinetic properties compared to previously reported agents. We assessed the pharmacokinetics, biodistribution, and CD38 specificity of [^{68}Ga]Ga-AJ206 in vitro and in vivo using multiple MM cell lines and xenografts with variable CD38 levels and in disseminated tumor models.

RESULTS.

Synthesis and characterization of AJ206

CD38 binding low molecular weight imaging agents have not been reported and high-affinity peptide therapeutics (IC_{50}<100 nM) were reported only recently which form the basis for our imaging agents **(Fig. 1**)(22). To test the applicability of those peptides for in vivo imaging, we selected a peptide with high hydrophilicity and a free amine for further functionalization. We synthesized a *2,2',2"-(1,4,7-triazacyclononane-1,4,7-triyl)triacetic acid* (NOTA)-conjugated peptide AJ206 with a poly ethylene glycol (PEG) linker to improve solubility (**Figure 1A**) and characterized by mass spectrometry (**Supplementary figure 1)**. We then tested its potential to bind human CD38 protein (hCD38) and MM cells with variable CD38 expression**.** AJ206 exhibited high affinity for CD38 with a dissociation constant (K_D) of 19.1 nM by Surface Plasmon Resonance (SPR) (**Figure 1B**).

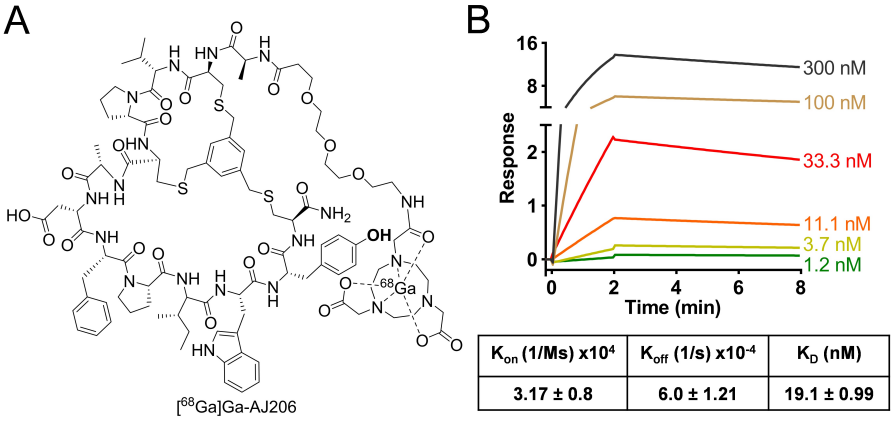

K_{on} (1/Ms) x10^4	K_{off} (1/s) x10^{-4}	K_D (nM)
3.17 ± 0.8	6.0 ± 1.21	19.1 ± 0.99

Figure 1. Structure and in vitro characterization of AJ206. A) Structure of a novel bicyclic peptide AJ206 having NOTA as bifunctional chelator for ^{68}Ga labeling B) Surface plasmon resonance (SPR) analysis showing affinity of AJ206 for CD38 using recombinant human CD38 protein; data is represented as mean±SEM (n=2)

Pharmacokinetics of [^{68}Ga]Ga-AJ206

We synthesized the radioactive analog of AJ206, [^{68}Ga]Ga-AJ206, by standard Ga-68 radiolabeling chemistry (**Supplementary scheme 3)** to evaluate the pharmacokinetics, biodistribution, and in vivo specificity(23). [^{68}Ga]Ga-AJ206 was obtained with decay corrected radiochemical yields of 92±10.5% (n=35) with >95% radiochemical purity and a specific activity (molar activity) of 10-15 GBq/µmol (270-400 mCi/µmol) (**Supplementary figure 3)**. The formulated [^{68}Ga]Ga-AJ206 dose remained stable for 2 h (**Supplementary figure 4**). Using immunodeficient NSG mice with MOLP8 human MM xenografts that are known to express CD38 (24), we evaluated [^{68}Ga]Ga-AJ206 in vivo. Whole body dynamic PET/MR images of those mice acquired over 90 min showed clear and high radiotracer accumulation in tumors as early as few minutes after injection, with a higher tumor contrast observed at 60 min due to background radiotracer clearance (**Figure 2A**). Kidney and bladder tissues had the highest radiotracer accumulation among normal tissues, consistent with the renal clearance mechanism for low-molecular-weight peptides, while radioactivity from other tissues, including liver, declined over 60 min (**Figure 2B**). These imaging data showed that [^{68}Ga]Ga-AJ206 exhibits in vivo kinetics and contrast desirable for an imaging agent. To verify the PET results, we conducted ex vivo biodistribution studies (**Table 1 and Supplementary table 1**). At 60 min, [^{68}Ga]Ga-AJ206 uptake in MOLP8 tumors peaked at 3.76±0.25% %ID/g. Blood pool activity exhibited consistent washout, with almost 95% of activity cleared by 60 min, and comparable radioactivity washouts were observed in all other non-specific tissues. As a result, the tumor-to-blood and tumor-to-muscle ratios were highest between 60 and 120 min (**Figure 2C and 2D, Table 1**). Thus, we chose the 60-minute time point for all further experiments because it provided good contrast and aligned with the standard PET imaging time frame. Furthermore, the imaging and biodistribution data indicated the potential of [^{68}Ga]Ga-AJ206 to detect CD38 levels non-invasively.

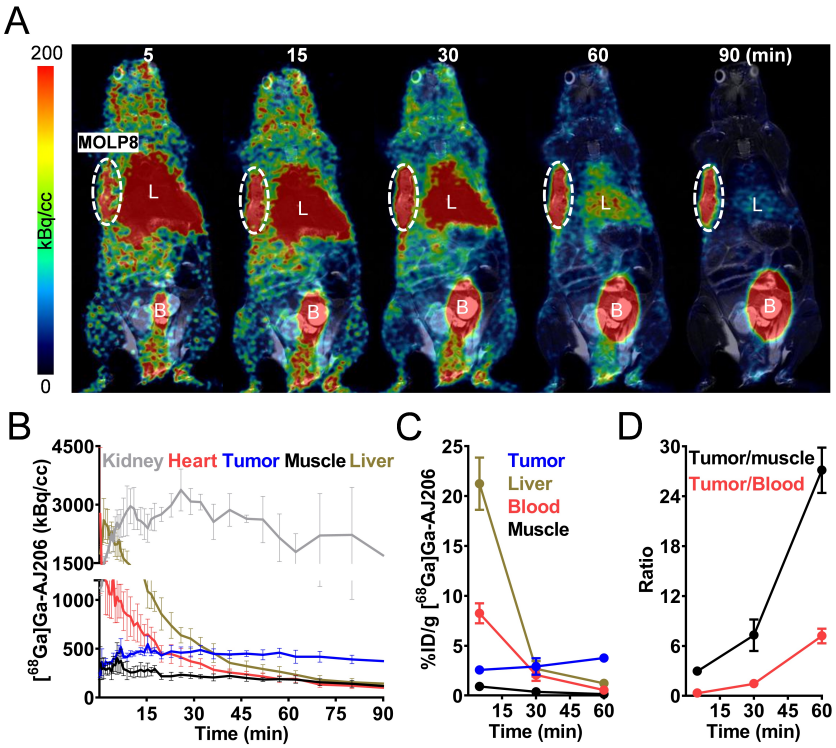

Figure 2. Pharmacokinetics of [^{68}Ga]Ga-AJ206 in NSG mice bearing MOLP8 tumor xenografts. A) Coronal sections of the fused dynamic PET/MR images showing [^{68}Ga]Ga-AJ206 distribution. Primary tumor is indicated by white circle. Mice were injected with ~ 7.4 MBq (~200 µCi) [^{68}Ga]Ga-AJ206. **B)** Time-activity curves of [^{68}Ga]Ga-AJ206 in the kidney, heart, liver, tumor and muscle. **C)** Uptake of [^{68}Ga]Ga-AJ206 in tumor, blood, liver and muscle derived from ex vivo biodistribution study. **D)** Tumor-to-muscle and tumor-to-blood ratios derived from biodistribution data. Data in panels **B, C** and **D** represent mean±SD (n=4 or 5) and mice were injected with ~ 740 kBq (~50 µCi) [^{68}Ga]Ga-AJ206 and sacrificed at different time-points after injection; L, Liver; B, Bladder.

Table 1. Kinetics of [^{68}Ga]Ga-AJ206 by ex vivo biodistribution study with MOLP8 tumor xenograft; data is presented as Mean±SEM (n=4 or 5) of %ID/g.

Tissues	5 min	30 min	60 min	120 min
Blood	8.25±0.50	2.07±0.30	0.56±0.09	0.05±0.01
Muscle	0.92±0.11	0.37±0.05	0.14±0.02	0.07±0.04
Tumor	2.58±0.18	2.91±0.84	3.76±0.25	1.46±0.02
Heart	3.13±0.27	0.83±0.18	0.29±0.03	0.05±0.01
Lungs	6.16±0.16	1.86±0.29	0.71±0.10	0.16±0.03
Liver	21.24±1.31	6.39±3.71	1.22±0.09	0.42±0.01
Spleen	2.28±0.50	0.75±0.14	0.39±0.03	0.17±0.02
Kidney	11.17±0.65	17.09±1.77	16.65±2.52	13.75±0.23
Stomach	1.08±0.07	0.51±0.06	0.25±0.06	0.03±0.01
Small intestine	1.95±0.08	0.59±0.14	0.65±0.09	0.18±0.04
Femur	1.42±0.09	0.65±0.08	0.28±0.07	0.07±0.01
Tumor/Muscle	2.94±0.47	7.28±1.89	27.12±2.73	27.37±18.55
Tumor/Blood	0.32±0.04	1.43±0.46	7.20±0.89	19.72±6.57

Human Radiation Dosimetry Estimates

Pharmacokinetic data obtained from biodistribution studies of MM1S tumor bearing mice was used to predict the residence time of [^{68}Ga]Ga-AJ206 in humans (**Table 2 and Supplementary table 1**). Residence time estimates were then employed as input to MIRDCalc to calculate the absorbed dose to organs from 68Ga using the ICRP adult female reference phantom (Table 2). The kidneys received the highest dose (0.13 rem/mCi), followed by the liver (0.06 rem/mCi), heart wall (0.05 rem/mCi), and lung (0.05 rem/mCi). Based on these results, a 30 mCi dose can be safely administered, with an estimated effective dose equivalent of less than 5 rem, to obtain PET images.

Table 2. Predicted residence times and absorbed doses of [^{68}Ga]Ga-AJ206 in human organs

Organs	Residence time (h)	Organ dose (rem/mCi)
Blood	0.09625	n/a
Muscle	0.04849	0.007548
Thymus	0.0002268	0.01961
Heart	0.001882	0.04995
Lung	0.01422	0.04884
Liver	0.04753	0.06142
Spleen	0.001063	0.026529
Pancreas	0.0005685	0.023791
Adrenals	0.0001171	0.03663
Kidney	0.02487	0.12691
Ovary	0.00007438	0.016613
Bladder	0.0007132	0.019869
Stomach (with contents)	0.0007474	0.020054
Small intestine (with contents)	0.004259	0.017501
Large intestine (with contents)	0.0006719	0.014652
Femur	0.003688	0.017242
Brain	0.0009592	0.003885

Confirmation of [^{68}Ga]Ga-AJ206 specificity in MM cell lines and xenografts with varying CD38 levels.

Next, we conducted an evaluation of the specificity of [^{68}Ga]Ga-AJ206 to detect varying levels of CD38 expression both in vitro and in vivo. Four MM cell lines (U266, RPMI, MM1S, and MOLP8) were incubated with [^{68}Ga]Ga-AJ206, and the amount of cell-bound radioactivity was measured. We observed that MOLP8 and U266 cells showed the highest and the least amount of radioactivity binding, respectively, while RPMI and MM1S cells demonstrated intermediate uptake (**Figure 3A**). We confirmed the specificity of [^{68}Ga]Ga-AJ206 binding by observing a significant reduction in radiotracer uptake ($P<0.0001$) when cells were incubated with a saturating concentration of a non-radioactive AJ206. To validate the invitro uptake, we performed flow cytometry analysis to measure cell surface expression and density, and western blot analysis to assess the total CD38 protein expression. Our results showed that highest cell surface receptor expression and density were observed in MOLP8 cells followed by RPMI and MM1S cells with the lowest expression in U266 cells (**Figure 3B and 3C**). Similarly, MOLP8 cells exhibited the highest total CD38 expression, followed by RPMI and MM1S cells, while U266 cells had the lowest (**Figure 3D**). We also performed a correlation analysis to investigate the relationship between [^{68}Ga]Ga-AJ206 uptake and CD38 receptor density, and found a strong correlation (R^2 = 0.9511), indicating that [^{68}Ga]Ga-AJ206 uptake in cells is CD38 specific (**Figure 3E**).

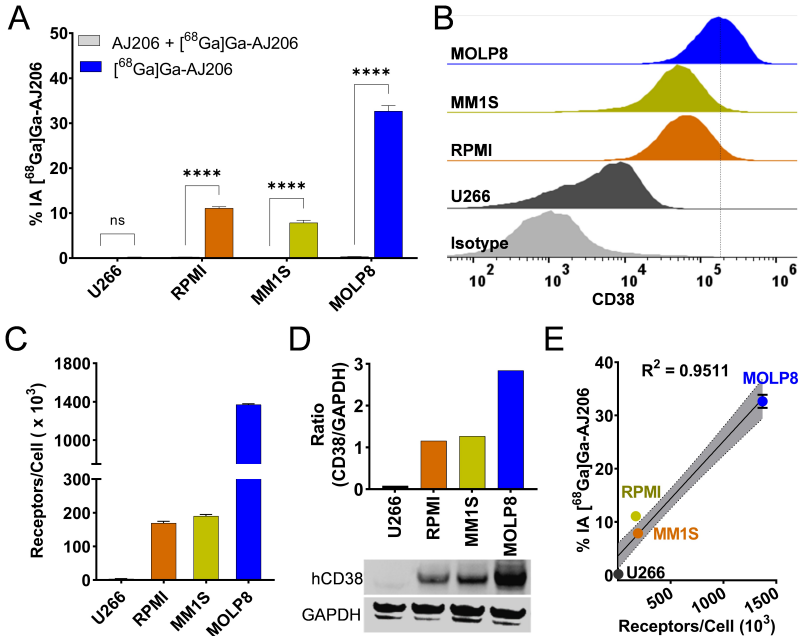

Figure 3. In vitro specificity of [^{68}Ga]Ga-AJ206 for CD38. A) [^{68}Ga]Ga-AJ206 binding (%IA) to different MM cells. Cells were incubated with [^{68}Ga]Ga-AJ206 at 4 °C for 1 hour. [^{68}Ga]Ga-AJ206 uptake is CD38 expression dependent, and co-incubation with 2 μM of unlabeled AJ206 (blocking dose) significantly reduced radiotracer uptake confirming CD38 specificity. **B)** Flow cytometry analysis of CD38 surface expression in MM cells. **C)** Cytometric-quantibrite assay to quantify CD38 receptor density in various MM cells. **D)** Representative western blot of total CD38 protein expression (bottom panel). Densiometric analysis of western blot preformed using Image J software and band intensities represented as a ratio of CD38 protein to GAPDH control (top panel), **E)** Correlation of [^{68}Ga]Ga-AJ206 uptake with CD38 receptor numbers; data in panels A, C and E are represented as mean±SD (n=3-4). ns, $p \geq 0.05$; ****, $p \leq 0.0001$ is by unpaired Student's t-test. Simple linear regression and Pearson coefficient were used in E.

To validate the in vitro results, we performed PET imaging studies of MM xenografts derived from the cell lines mentioned above, using [^{68}Ga]Ga-AJ206. PET images were acquired at 60 min and showed highest radioactivity accumulation in MOLP8 tumors, followed by MM1S and RPMI tumors, and least accumulation in U266 tumors (**Figure 4A**). To corroborate the PET data, we performed IHC staining of the same xenografts for CD38 and found intense staining in MOLP8 xenografts and least in U266 tumors (**Figure 4B**). Additionally, we conducted ex vivo biodistribution studies to further validate the imaging findings. We found that the tumor uptake was consistent with the in vitro and PET results, with the highest uptake observed with MOLP8 tumors (3.76±0.25 %ID/g), followed by MM1S (2.48±0.17 %ID/g) and RPMI (1.7±0.36). On the other hand, U266 tumors showed less than 0.25 %ID/g of [^{68}Ga]Ga-AJ206, which is in line with their low CD38 levels. The tumor-to-muscle and tumor-to-blood ratios showed similar trends with respect to CD38 status (**Figure 4C**), and background tissues showed no significant differences between tumor models (**Table 3**). Furthermore, we demonstrated the specificity of [^{68}Ga]Ga-AJ206 for CD38 by co-administering 2 mg/kg non-radioactive AJ206 with the radiotracer, which significantly reduced radioactivity uptake in MM1S xenografts ($P<0.05$) (**Figure 4D and 4E**). These in vitro and in vivo data together demonstrate the potential of [^{68}Ga]Ga-AJ206 for non-invasive detection of varying levels of CD38 expression in vivo.

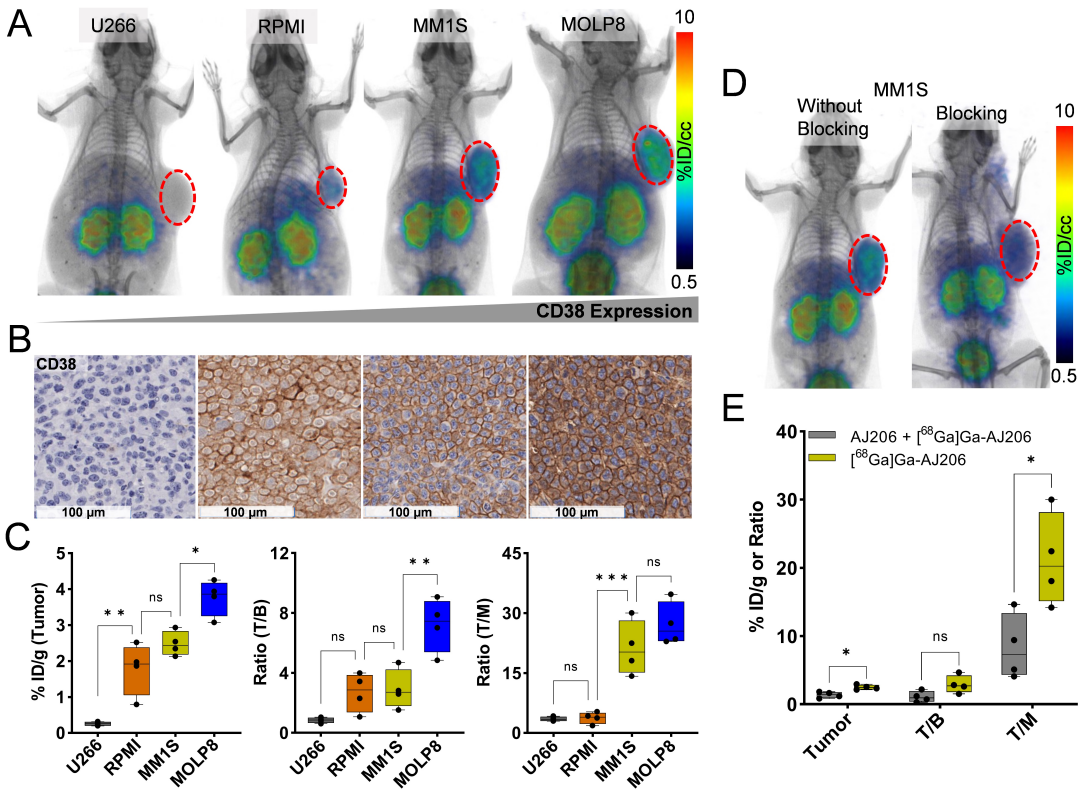

Figure 4. In vivo specificity of [^{68}Ga]Ga-AJ206 for CD38 in NSG mice with MM tumor xenografts. A) Whole-body PET/CT images of different human MM xenografts at 60 min after the injection of the radiotracer. Mice were injected with ~ 7.4 MBq (~200 µCi) [^{68}Ga]Ga-AJ206. **B)** IHC staining for CD38 expression in MM xenografts. **C)** [^{68}Ga]Ga-AJ206 uptake quantification in different MM xenografts by ex vivo biodistribution at 60 min after injection. **D)** PET/CT images of MM1S tumor xenograft-bearing mice with [^{68}Ga]Ga-AJ206, with and without pre-administration of a blocking dose (50 µg of AJ206). **E)** [^{68}Ga]Ga-AJ206 quantification in tumors by ex vivo biodistribution in mice treated with and without a blocking dose; data in figure **C**, and **E** are shown as box and whisker plots showing all data points (n=4-5). Ordinary one-way ANOVA using multiple comparison test in C and multiple unpaired t-test in E. ns, $p \geq 0.05$; *, $p \leq 0.05$; ** $p \leq 0.01$; ***, $p \leq 0.001$.

Table 3. Ex vivo biodistribution study with various MM tumor xenografts with [^{68}Ga]Ga-AJ206 at 60 min post-injection; data is presented as mean±SEM (n=4 or 5) of %ID/g. *, tissue not available.

Tissues	U266	RPMI	MM1S	MM1S with Blocking	MOLP8
Blood	0.32±0.06	0.98±0.48	0.97±0.18	2.17±1.17	0.56±0.09
Muscle	0.08±0.01	0.49±0.07	0.13±0.02	0.21±0.07	0.14±0.02
Tumor	0.25±0.03	1.78±0.36	2.48±0.17	1.37±0.22	3.76±0.25
Heart	0.15±0.02	0.63±0.21	0.29±0.03	0.33±0.03	0.29±0.03
Lung	0.42±0.04	1.00±0.26	0.67±0.07	0.94±0.09	0.71±0.10
Liver	0.78±0.06	1.27±0.30	1.38±0.04	1.45±0.26	1.22±0.09
Spleen	0.24±0.01	1.09±0.15	0.41±0.05	0.90±0.45	0.39±0.03
Pancreas	*	0.48±0.15	0.19±0.03	0.64±0.39	*
Kidney	21.51±2.68	17.81±3.48	14.09±0.57	15.91±1.12	16.65±2.52
Stomach	0.39±0.30	0.45±0.07	0.32±0.21	1.01±0.56	0.25±0.06
Small intestine	0.16±0.01	0.59±0.25	0.20±0.10	0.87±0.50	0.65±0.09
Femur	0.13±0.02	*	0.33±0.12	0.25±0.09	0.28±0.07
Tumor/Muscle	3.43±0.28	3.72±0.73	21.17±3.40	8.31±2.41	27.12±2.73
Tumor/Blood	0.83±0.09	2.69±0.65	2.90±0.65	1.08±0.40	7.20±0.89

Validation of [^{68}Ga]Ga-AJ206 specificity in disseminated MM disease models.

We next conducted a study to evaluate the potential of [^{68}Ga]Ga-AJ206 in visualizing disease in bone marrow and soft tissues for non-invasive monitoring of high-risk MM phenotypes. Extramedullary manifestation (EMD) and plasma cell leukemia (PLC) are two aggressive clinical presentations of MM that exhibit high relapse rates. EMD presents with infiltration in other organs, such as lymph nodes, liver, lungs, and central nervous system, while PLC is characterized by free circulation of MM cells in the blood. To achieve this, we generated a disseminated disease model by intravenously injecting luciferase expressing MM1S (**Figure 5A**) or MOLP8 cells into NSG mice. [^{68}Ga]Ga-AJ206 PET images showed specific accumulation of radioactivity in bone lesions in both MM1S and MOLP8 tumor models (**Figure 5B and D**), which was further validated by bioluminescence imaging in MM1S model (Figure 5A) and ex vivo PET imaging in MOLP8 model (**Figures 5D**). Metastases in lungs were also detectable through [^{68}Ga]Ga-AJ206 PET imaging (**Figure 5B**). The lung and bone tissue analysis using flow cytometry and IHC showed high intensity for CD38, a marker for MM cells (**Figure 5C and E**). Furthermore, analysis of bone lesions from MM1S and MOLP8 models showed differential uptake, indicating that different CD38 levels can be differentiated by [^{68}Ga]Ga-AJ206 PET (**Figure 5F and 5G**). We also extracted cells from the bone marrow of those mice, which showed high CD38 expression, thus confirming that the observed uptake is indeed CD38 specific (**Figures 5H**). These results indicate that [^{68}Ga]Ga-AJ206 could benefit high-risk MM phenotypes such as EMD and PLC by detecting and monitoring the disease in soft tissues and bone marrow. In conclusion, these results demonstrate that [^{68}Ga]Ga-AJ206 has potential as a non-invasive imaging agent for detecting and monitoring MM in soft tissues and bone marrow, complementing existing methods for non-invasive monitoring of high-risk MM phenotypes.

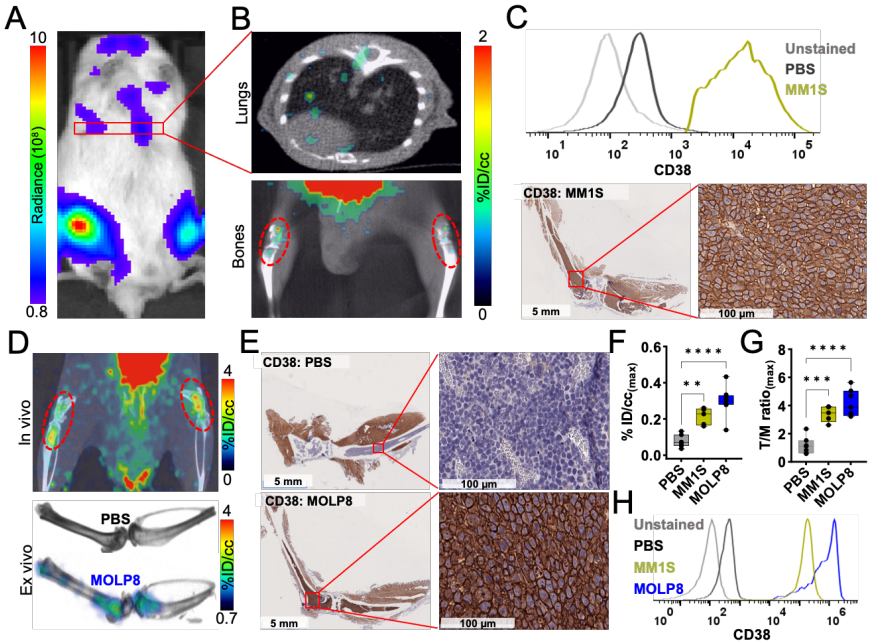

Figure 5. Validation of [^{68}Ga]Ga-AJ206 specificity for CD38 in disseminated disease models. A) IVIS-bioluminescence image of luciferase expressing MM1S disseminated tumor model (i.v) showing luciferase expression in lower limbs, unit of radiance is watt per steradian per square metre ($W \cdot sr^{-1} \cdot m^{-2}$) **B)** In vivo uptake of [^{68}Ga]Ga-AJ206 in lungs and bones **C)** Flow cytometry analysis of CD38 expression in lungs harvested from of MM1S-Luc cells injected mice. Lungs from PBS treated mice were used as controls (Top). IHC staining of bones to validate CD38 expression (bottom). **D)** In vivo and ex vivo [^{68}Ga]Ga-AJ206-PET images of lower limbs of MOLP8 injected (i.v) animals. **E)** IHC images of MOLP8 bone marrow tumor and PBS treated animals confirming CD38 expression **F)** Flow cytometry analysis of CD38 expression in cells extracted from bone marrows of PBS, MM1S-Luc and MOLP8 cell injected mice. **G)** Quantification of PET signals in the bone marrow of PBS, MM1S and MOLP8 injected animals **H)** Tumor/muscle ratios of PET measures in the bone marrows of PBS, MM1S and MOLP8 injected animals; data in figure G and H are shown as box and whisker plots showing all data points (n=7 in PBS, n=5 in MM1S and n=8 in MOLP8). Ordinary one-way ANOVA using multiple comparison test. ** $p \leq 0.01$; ***, $p \leq 0.001$; ****, $p \leq 0.0001$.

DISCUSSION.

In this study, we demonstrated that a new gallium-68 labeled radiotracer, [^{68}Ga]Ga-AJ206, exhibits high affinity for CD38 and optimal pharmacokinetics with excellent image contrast within 60 minutes after administration, aligning with standard clinical workflow. Through various tumor models, we confirmed that [^{68}Ga]Ga-AJ206 detects varying levels of CD38 expression and differentiates CD38 levels in bone lesions in disseminated disease models. As treatments for MM improve, more people are living with the disease. Continuous therapy has consistently been associated with the best outcomes. However, there are efforts underway to tailor or taper treatment in patients who have little or no detectable minimal residual disease to reduce toxicity. As a result, the accurate detection of disease in the whole body and small amounts of disease will become increasingly important for this growing patient population. Our findings indicate that [^{68}Ga]Ga-AJ206 has the potential to be a useful radiotracer in clinical settings for monitoring therapy response and disease progression in MM.

Taking advantage of high CD38 expression in MM, several CD38-targeting therapies have been developed or are in different phases of clinical development (21). These include monoclonal antibodies such as daratumumab and Isatuximab, which are approved for treating MM, as well as other forms of therapies such as ADCs, T-cell engagers, and CAR-T cells (21,25). Responses to anti-CD38 mAbs has been linked to CD38 receptor density and MM cells with higher levels of CD38 expression are more susceptible to anti-CD38-mediated therapeutic effects compared to low CD38 expression levels (21,26-28). Also, there is substantial heterogeneity in response among patients treated with these therapies and more than half of the patients do not respond to single-agent daratumumab (27,29-31). For example, daratumumab has been shown to induce durable responses in heavily pretreated patients, but a majority of the responding patients eventually develop progressive disease during daratumumab monotherapy. Also, primary resistance to daratumumab has been linked to CD38 receptor density (20). Those clinical observations suggests that real-time, whole-body measurements of CD38 expression using molecularly targeted PET radiotracers could provide more accurate information for guiding anti-CD38 therapies in MM than current single-time point, single-lesion flow cytometry-based measurements. Moreover, non-invasive CD38 monitoring is expected to have a broader application across different disease states of MM, as well as be applicable to a range of malignancies with known CD38 involvement, such as NK/T cell lymphoma, T-cell acute lymphoblastic leukemia, primary effusion lymphoma, and immunoglobulin light-chain amyloidosis.

Considering the importance of CD38 expression in MM, radiolabeled and fluorescence conjugates of daratumumab has been tested in preclinical models and patients. Several clinical trials are ongoing to capture the heterogeneity in CD38 levels in the whole body using radiolabeled analogs of the FDA approved anti-CD38 antibodies (mAbs). Radiolabeled anti-CD38 mAb (^{89}Zr-daratumumab) localization to the osseous MM sites was visualized by PET with appreciable contrast by day 7 (15). In another clinical trial using copper-64 daratumumab lesions that were ^{18}F-FDG negative but positive in CD38-PET were found to be positive for MM involvement on biopsy (32), indicating the potential for CD38-PET for improved disease burden assessment. Our peptide tracers are small, synthetic (~2.1 kDa), exhibit tractable pharmacokinetics, and take advantage of the inherent sensitivity of PET and the higher contrast resolution characteristics of ^{68}Ga. As such, we observed the potential of [^{68}Ga]Ga-AJ206 to detect varying CD38 levels in a variety of tumor models that is corroborated by CD38 IHC. Furthermore, our results suggest that CD38 specific low molecular weight diagnostic agents may have a number of applications in MM, including assessing total CD38 levels, predicting response to therapy and determining CD38 occupancy by mAbs, similar to what has been shown by us for PD-L1 therapeutics (33-35). Also, clinical trial evaluation of ATRA induced changes in CD38 expression was evaluated in peripheral blood samples but not in bone marrow samples due to the invasive nature of the procedure (36). The potential of [^{68}Ga]Ga-AJ206 to quantify therapy induced changes in CD38 levels suggest that non-invasive monitoring of CD38 levels may find use in monitoring therapy.

MATERIALS AND METHODS.

Chemicals. NOTA-NHS ester was purchased from CheMatech, and all Fmoc protected amino acids, TIPS, HOBT, and HBTU were obtained from Chem-impex. Fmoc-PEG-COOH and tBu3-DOTA-COOH were purchased from Ambeed, while DIPEA, TFA, DODT, TBMB, and DMF were obtained from Sigma-Aldrich.

Synthesis of AJ205. AJ205 was chemically synthesized using Liberty Blue CEM automatic peptide synthesizer employing Fmoc based solid-phase peptide synthesis on Rink Amide resin in a 0.1 mmol scale (**Supplementary scheme 1**). Coupling reaction was carried out using Oxyma (0.5 mmol), DIC (1 mmol) and Fmoc-AA-OH (0.5 mmol) in DMF with microwave assisted reaction for 2 min. Fmoc group was deprotected using 20% piperidine in DMF (3 mL) for 1 min with microwave assistance. Next, PEG linker was incorporated using HBTU (0.5 mmol), HOBT (0.5 mmol), DIPEA (0.5 mmol) and Fmoc-PEG_3-COOH (0.5 mmol) in DMF at room temperature for 1.5 h and then Fmoc group was deprotected using 20% piperidine (4 mL) in DMF for 40 min at room temperature. Once the sequence was completed on the resin, the peptidyl-resin was treated with 4 mL of cleavage cocktail (TFA:TIPS:DODT:H_2O; 92.5:2.5:2.5:2.5) for 4 h at room temperature. The cleaved reaction mixture was precipitated with diethyl ether to obtain the linear peptide as a white solid.

For the cyclization, the linear peptide (98 mg, 0.06 mmol) was dissolved in 100 mL of water:acetonitrile (1:1) and treated with an aqueous solution of tris(2-carboxyethyl)phosphine (TCEP) (115 mg, 0.4 mmol) followed by Et_3N (400 µL, 2.9 mmol). 1,3,5-Tris(bromomethyl)benzene (TBMB) (34 mg, 0.1 mmol) was dissolved in 2 mL of acetonitrile and added slowly to the reaction mixture over an hour. The reaction mixture was stirred at room temperature for 24 h and quenched with TFA. The volatiles were removed and the crude mixture was purified on a reversed-phase high-performance liquid chromatography (RP-HPLC) system using a preparative C-18 Phenomenex column (5 mm, 21.5 x 250 mm Phenomenex, Torrance, CA). The HPLC condition was gradient elution starting with 10% acetonitrile: water (0.1% TFA) and reaching 60% acetonitrile: water (0.1% TFA) in 40 min at a flow rate of 8 mL/min. The product AJ205 was collected at RT ~28.2 min. Acetonitrile was evaporated under reduced pressure and lyophilized to form an off-white powder with a 37% yield (40 mg). The sequence of the AJ205 peptide is NH_2-PEG_3-ACVPCADFPIWYC-NH_2 with TBMB-based cyclization. This peptide was characterized by MALDI-TOF-MS. The theoretical chemical formula is $C_{87}H_{118}N_{16}O_{20}S_3$ with an exact mass of 1802.79 and a molecular weight of 1804.17. The theoretical MALDI-TOF-MS mass $[M + H]^+$ was 1803.8; the observed ESI-MS mass $[M + H]^+$ was 1804.0.

Synthesis of AJ206. To a stirred solution of AJ205 (2.1 mg, 1.2 µmoles) in 200 µL of DMF in a reaction vial, NOTA-NHS ester (2.0 mg, 2.8 µmoles) and DIPEA (5 µL, 25 µmoles) were added and stirred at room temperature for 3 h (**Supplementary scheme 2**). DMF was evaporated using a rotary evaporator under reduced pressure and the residual product was purified on a RP-HPLC system using a semi-preparative C-18 Luna column (5 mm, 10 x 250 mm Phenomenex, Torrance, CA). The HPLC condition was gradient elution started with 5% acetonitrile: water (0.1% TFA) and reached at 95% acetonitrile: water (0.1% TFA) in 20 min at a flow rate of 5 mL/min. The product AJ206 was collected at RT ~11.8 min. Acetonitrile was evaporated under reduced pressure and lyophilized to form an off-white powder with a 52% yield, which was characterized by MALDI-TOF-MS. The theoretical chemical formula of AJ206 is $C_{99}H_{137}N_{19}O_{25}S_3$ with an exact mass of 2087.92 and molecular weight of 2089.47. The theoretical MALDI-TOF-MS mass $[M + H]^+$ is 2088.9, and the observed ESI-MS mass $[M + H]^+$ is 2089.1.

Affinity measurements by surface plasmon resonance (SPR). The affinity of AJ206 for hCD38 and mCD38 was evaluated by SPR. The experiments were conducted using a Biacore T200 instrument with a CM5 chip at 25 °C. The ligands used were His-Tagged human CD38 (R&D systems, catalog # 2404-AC, 43 kDa, 0.5 mg/ml stock concentration) and mouse CD38 proteins (R&D systems, catalog # 4947-AC, 40 kDa, 1.81 mg/ml stock concentration), which were immobilized onto the CM5 chip. AJ206 (2089.2 Da, 10 mM stock concentration) was used as the analyte, which flowed over the ligand immobilized surface. FC2 was used as the experimental flow cell, while FC1 served as the reference. Anti-His antibody (1 mg/ml stock concentration) was immobilized on both FC1 and FC2 using standard amine coupling chemistry. The immobilization running buffer used was PBS-P (20 mM phosphate buffer pH 7.4, 137 mM NaCl, 2.7 mM KCl, 0.05% v/v surfactant P20). Human CD38 was captured onto FC2 at a level of ~860 RU, with a 1:20 dilution and 25 µg/ml diluted concentration in PBS-P. Mouse CD38 was captured onto FC4 at a level of 1360 RU, with a 1:50 dilution and 36.2 µg/ml diluted concentration in PBS-P. The theoretical Rmax values were calculated based on the captured response values

and are presented in table 1, assuming a 1:1 interaction mechanism. Overnight kinetics were performed for all analytes in the presence of PBS-P+1% DMSO. The flow rate of all analyte solutions was maintained at 50 µL/min. The contact and dissociation times used were 120s and 360s, respectively. Surface regeneration was achieved by injecting glycine pH 1.5 for 20 seconds, which takes away all captured ligands onto FC2. Fresh ligands were captured at the beginning of each injection cycle. The analyte concentrations injected ranged from 300 nM down to 1.2 nM with three-fold serial dilutions, and all analytes were injected in triplicate.

Ligand	FC	Analyte	Ligand Binding (RU)	MWL (Da)	MWA(Da)	Stochiometric Ratio	R_{max}
Human CD38	2	AJ206	860	40000	2089.6	1:1	39.2
Mouse CD38	4	AJ206	1360	40000	2089.6	1:1	71.0

Synthesis of [^{nat}Ga]Ga-AJ206. The synthesis of [^{nat}Ga]Ga-AJ206 was carried out by adding 10 µL of aqueous 0.1M ^{nat}GaCl3 solution and 0.6 mL of 0.1 M HCl to a stirred solution of AJ206 (0.1 mg, 0.05 µmoles) in 200 µL of 1M NaOAc buffer (pH 5.0) in a reaction vial. The reaction mixture was incubated at 65 °C for 30 min and then purified on a RP-HPLC system using a semi-preparative C-18 Luna column (5 mm, 10 x 250 mm Phenomenex, Torrance, CA). The HPLC gradient elution condition started with 5% acetonitrile: water (0.1% TFA) and reached at 95% acetonitrile: water (0.1% TFA) in 20 min at a flow rate of 5 mL/min. The product [^{nat}Ga]Ga-AJ206 was collected at RT ~11.8 min. The acetonitrile was evaporated under reduced pressure and lyophilized to form an off-white powder, which was characterized by MALDI-TOF-MS. The theoretical chemical formula is $C_{99}H_{134}GaN_{19}O_{25}S_3$ with an exact mass of 2153.82 and a molecular weight of 2156.17. The theoretical MALDI-TOF-MS mass $[M + H]^+$ was 2154.8, and the observed ESI-MS mass $[M + H]^+$ was 2154.1.

Synthesis of [^{68}Ga]Ga-AJ206. The ^{68}Ge/^{68}Ga generator was manually eluted using 6 mL of 0.1M HCl (Ultrapure trace-metal-free) in four different fractions (2.4 mL, 1 mL, 1 mL, and 1.4 mL). To a microcentrifuge vial (1.5 mL) containing 200 µL of 1 M NaOAc buffer (pH = 5) and 20 µg of AJ206 (10 nmoles), 3-4 mCi of $^{68}GaCl_3$ in 0.6 mL from the second fraction was added. The reaction mixture was incubated for 12 min at 65 °C in a temperature-controlled heating block and purified on a RP-HPLC system using a semi-preparative C-18 Luna column (5 mm, 10 x 250 mm Phenomenex, Torrance, CA). The HPLC condition was gradient elution starting with 5% acetonitrile: water (0.1% TFA) and reaching 95% acetonitrile: water (0.1% TFA) in 20 min at a flow rate of 5 mL/min. The radiolabeled product [^{68}Ga]Ga-AJ206 was collected at RT ~11.8 min, with decay-corrected radiochemical yield of 92±10.5 % (n=48). The desired radiolabeled fraction was concentrated under a stream of N_2 at 60 °C, formulated in 10% EtOH in saline, and used for in vitro and in vivo studies. The whole radiolabeling process was completed in approximately 35 min. Quality control, stability studies, and chemical identity were also performed on the same HPLC system using the same HPLC gradient as described above.

Cell Culture. MOLP8 cells were purchased from Deutsche Sammlung von Mikroorganismen und Zellkulturen (DSMZ), Germany, under the material transfer agreement guidelines with Johns Hopkins University. Other cell lines (U266, RPMI8226, MM1S) were gifted from a collaborator. Prior to the start of the experiments, all cell lines were authenticated by STR profiling at the Johns Hopkins Genetic Resources Facility. Routine Mycoplasma testing was conducted, and the cell lines were passaged for no more than three months. New cultures were initiated from vials of frozen cells. All cell lines (U266, RMPI8226, MM1S, MM1S-Luc, and MOLP8) were cultured in the recommended media and maintained in an incubator at 37 °C in an atmosphere containing 5% CO2. All cells were supplemented with fetal bovine serum, 1% P/S antibiotics, and 1mM L-Glutamine.

In vitro cellular binding assays. In vitro binding assays were conducted to determine the binding of [^{68}Ga]Ga-AJ206 to U266, RPMI8226, MM1S, and MOLP8 cells. Approximately 1 µCi of [^{68}Ga]Ga-AJ206 was incubated with 1×10^6 cells for 60 min at 4 °C. After incubation, cells were washed three times with ice-cold PBS containing 0.1% tween-20 and counted on an automated gamma counter (1282 Compugamma CS, Pharmacia/LKB Nuclear, Inc., Gaithersburg, MD). Blocking was performed with 2 µM of AJ206 to demonstrate CD38-specific cellular binding of [^{68}Ga]Ga-AJ206. All cellular uptake studies were performed in quadruplicate for each cell line and repeated three times.

Flow cytometry analysis of CD38 expression. To evaluate CD38 surface expression, cells ($1x10^6$) were stained with PE-labelled anti-human CD38 monoclonal antibody (clone HB-7, BioLegend Cat # 356604) in FACS

buffer (0.5% FBS with 2 mM EDTA) for 30 min on ice. After washing and resuspending in FACS buffer, data was acquired on a BD Accuri C6 plus flow cytometer and analyzed using FlowJo software. Receptor density measurements were performed using Quantibrite Beads (BD Biosciences, cat #340495), which contain four levels of phycoerythrin (PE) per bead. Gates were drawn on Low, Medium Low, Medium High, and High PE binding beads, and the geometric mean (FL-2 A: PE-A) from these populations was correlated with the lot-specific PE molecule/bead on a logarithmic scale. This correlation was used to translate cell population geometric mean to receptor/cell for the respective cell type.

Western blotting. To assess CD38 protein expression in MM cells, lysed cells were denatured using Laemmli SDS sample buffer with beta-mercaptaethanol, loaded onto SDS-PAGE gels, and transferred to PVDF membranes. Blots were probed with rabbit monoclonal anti-human CD38 antibody (Clone RM388, Thermo Scientific, cat# MA5-36061) after blocking with 5% BSA. GAPDH was used as a loading control (Rabbit polyclonal, Clone D16H11, CST, cat# 5174). Blots were incubated overnight at 4°C, washed, and incubated with anti-rabbit IgG, HRP-linked secondary antibody (CST cat #7074) to detect binding. Immunoreactivity was detected using super signal west Pico plus Chemiluminescent substrate (Thermo Scientific) and analyzed on iBright CL1500 Imaging System using Chemidoc scanner.

Mouse tumor models for PET imaging and Ex-vivo biodistribution studies. Animal studies were performed under Johns Hopkins University ACUC-approved protocols. Male and Female NSG mice (5-6 weeks old) were used to establish xenografts by administering 3 million cells (50% Corning Matrigel) subcutaneously to form various tumor models within 3-4 weeks. Imaging or biodistribution studies (n=3-5) were conducted on mice with tumor volumes of 100-200 mm^3. Orthotopic tumor engraftment was developed by injecting 4-5 million cells in saline intravenously for MOLP8 and MM1S models (n=4-5). Luciferase expressing MM1S cell line (MM1S-Luc) was used to monitor cancer cell dissemination in the body. Tumor establishment was confirmed by injecting D-Luciferin intraperitoneally (150 mg/kg) and imaging mice after 10 min in IVIS bioluminescence imaging system. Bone marrow tumors were ready for imaging after 25-30 days of implantation.

Evaluation of pharmacokinetics of [^{68}Ga]Ga-AJ206. Dynamic PET images were acquired on a Simultaneous 7T Bruker PET-MR scanner to evaluate the pharmacokinetics of [^{68}Ga]Ga-AJ206. Mice bearing MOLP8 tumor xenografts were anesthetized under 2.5% isoflurane and a catheter was fixed in the tail vein before being secured on the PET-MR bed. A dose of ~250 µCi (9.3 MBq) of [^{68}Ga]Ga-AJ206 was administered intravenously and whole-body PET dynamic scans were performed starting from -1 to 5 min in 30-second intervals, followed by scans at 5-15 min in 1-minute intervals, 15-30 min in 3-minute intervals, 30-60 min in 5-minute intervals, and 60-90 min in 10-minute intervals. The acquired PET data were reconstructed and corrected for radioactive decay and dead time using ParaVision 360 V2 by Bruker. The %ID per cc values were obtained by drawing ROI on the tumor, muscle, and kidney using PMOD software, and image fusion and visualization were also performed using PMOD software.

PET-CT imaging of mouse xenografts. Mice bearing flank tumors and disseminated disease were injected with [^{68}Ga]Ga-AJ206 and PET images were acquired 60 minutes after injection of the radiotracer. Images were acquired in 2 bed positions for a total of 10 minutes using an ARGUS small-animal PET/CT scanner. Images were reconstructed using 2D-OSEM and corrected for radioactive decay and dead time. Image fusion, visualization, and 3D rendering were accomplished using Amira 2020.3.1. PET images were quantified by drawing ROI on tissues using Amide 1.0.6 and reported as %ID/cc.

Ex vivo biodistribution. Mice with 100-200 mm^3 tumor volume were used for ex vivo biodistribution studies. For radiotracer pharmacokinetics studies, mice with MOLP8 tumor xenograft received ~80 µCi (2.96 MBq) [^{68}Ga]Ga-AJ206 and were sacrificed at pre-determined time points (5, 30, 60 and 120 min). Similarly, for dosimetry study, mice with MM1S tumor xenograft received ~80 µCi (2.96 MBq) [^{68}Ga]Ga-AJ206 and were sacrificed at pre-determined time points (5, 30, 60, 90 and 120 min). All other mice were injected with ~50µCi (1.85 MBq) [^{68}Ga]Ga-AJ206 and were sacrificed at 60 min. The selected tissues were collected, weighed, counted, and their %ID/g values calculated for biodistribution analysis. The tissues included blood, muscle, tumor, thymus, heart, lung, liver, pancreas, stomach, small intestine, large intestine, spleen, adrenals, kidney, bladder, femur, and brain.

Harvesting of tissues for immunohistochemistry and flow cytometry. After the imaging study, mice were humanely euthanized and their tissues Including inflated lungs, and tumors were fixed in 4% paraformaldehyde and sent to Oncology tissue services (OTS) at JHU. Tissue sections of 4 μm thickness were prepared from paraffin-embedded tissues. Bones that were harvested were fixed and decalcified for 15 days in 10% EDTA on a slow-speed rocking shaker.

For flow cytometric analysis, single-cell suspensions were prepared from bone marrow and lungs. Femurs were properly blenched and cut from the epiphysis, and cells were collected directly in tubes. Lungs were chopped and digested in a buffer containing collagenase and DNase, incubated at 37°C for 30 minutes, and strained through a 40um cell strainer. Cell pellets were lysed in RBC lysis buffer, and live/dead staining was conducted using Near Infra-red 780 dye and CD38 staining, as previously described.

Immunohistochemistry. To perform immunohistochemistry, the tissue slides were deparaffinized by baking at 60°C and washing with xylene and alcohol. Antigen retrieval was carried out using citrate buffer (pH 6.0, 95-100°C, 20 min) and the endogenous peroxidase and alkaline phosphatase activity was blocked using BioXALL. The primary anti-human CD38 antibody was applied at a dilution of 1:250 and incubated overnight at 4°C (Thermo Scientific clone RM388 Cat# MA5-36061). After washing with PBS, the secondary antibody, Signalstain Boost IHC Detection Reagent (HRP), was applied and incubated for 30 min at room temperature. The slides were washed and developed using ImmPACT DAB substrate. After washing, the slides were counterstained with Mayer's Hematoxylin for 1 min, dehydrated using alcohol and xylene, and then cover slipped.

Statistical analysis: All statistical analyses were performed using Prism 9.0 Software (GraphPad Software, La Jolla, CA). Unpaired Student's t-test and one- or two-way ANOVA were utilized for column, multiple column, and grouped analyses, respectively. Statistical significance was set at $P<0.05$ and $p \geq 0.05$ is ns, $p \leq 0.05$ is *, $p \leq 0.01$ is **, $p \leq 0.001$ is ***, $p \leq 0.0001$ is ****. Correlation was performed using simple linear regression without keeping the term constant at zero.

Figure legends:

Figure 1. Structure and in vitro characterization of AJ206. A) Structure of a novel bicyclic peptide AJ206 having NOTA as bifunctional chelator for ^{68}Ga labeling B) Surface plasmon resonance (SPR) analysis showing affinity of AJ206 for CD38 using recombinant human CD38 protein; data is represented as mean±SEM (n=2)

Figure 2. Pharmacokinetics of [^{68}Ga]Ga-AJ206 in NSG mice bearing MOLP8 tumor xenografts. A) Coronal sections of the fused dynamic PET/MR images showing [^{68}Ga]Ga-AJ206 distribution. Primary tumor is indicated by white circle. Mice were injected with ~ 7.4 MBq (~200 µCi) [^{68}Ga]Ga-AJ206. **B)** Time-activity curves of [^{68}Ga]Ga-AJ206 in the kidney, heart, liver, tumor and muscle. **C)** Uptake of [^{68}Ga]Ga-AJ206 in tumor, blood, liver and muscle derived from ex vivo biodistribution study. **D)** Tumor-to-muscle and tumor-to-blood ratios derived from biodistribution data. Data in panels **B, C** and **D** represent mean±SD (n=4 or 5) and mice were injected with ~ 740 kBq (~50 µCi) [^{68}Ga]Ga-AJ206 and sacrificed at different time-points after injection; L, Liver; B, Bladder.

Figure 3. In vitro specificity of [^{68}Ga]Ga-AJ206 for CD38. A) [^{68}Ga]Ga-AJ206 binding (%IA) to different MM cells. Cells were incubated with [^{68}Ga]Ga-AJ206 at 4 °C for 1 hour. [^{68}Ga]Ga-AJ206 uptake is CD38 expression dependent, and co-incubation with 2 µM of unlabeled AJ206 (blocking dose) significantly reduced radiotracer uptake confirming CD38 specificity. **B)** Flow cytometry analysis of CD38 surface expression in MM cells. **C)** Cytometric-quantibrite assay to quantify CD38 receptor density in various MM cells. **D)** Representative western blot of total CD38 protein expression (bottom panel). Densiometric analysis of western blot preformed using Image J software and band intensities represented as a ratio of CD38 protein to GAPDH control (top panel), **E)** Correlation of [^{68}Ga]Ga-AJ206 uptake with CD38 receptor numbers; data in panels A, C and E are represented as mean±SD (n=3-4). ns, $p \geq 0.05$; *, $p \leq 0.05$; ** $p \leq 0.01$; ***, $p \leq 0.001$; ****, $p \leq 0.0001$ is by unpaired Student's t-test. Simple linear regression and Pearson coefficient were used in E.

Figure 4. In vivo specificity of [^{68}Ga]Ga-AJ206 for CD38 in NSG mice with MM tumor xenografts. A) Whole-body PET/CT images of different human MM xenografts at 60 min after the injection of the radiotracer. Mice were injected with ~ 7.4 MBq (~200 µCi) [^{68}Ga]Ga-AJ206. **B)** IHC staining for CD38 expression in MM xenografts. **C)** [^{68}Ga]Ga-AJ206 uptake quantification in different MM xenografts by ex vivo biodistribution at 60 min after injection. **D)** PET/CT images of MM1S tumor xenograft-bearing mice with [^{68}Ga]Ga-AJ206, with and without pre-administration of a blocking dose (50 µg of AJ206). **E)** [^{68}Ga]Ga-AJ206 quantification in tumors by ex vivo biodistribution in mice treated with and without a blocking dose; data in figure **C**, and **E** are shown as box and whisker plots showing all data points (n=4-5). Ordinary one-way ANOVA using multiple comparison test in C and multiple unpaired t-test in E. ns, $p \geq 0.05$; *, $p \leq 0.05$; ** $p \leq 0.01$; ***, $p \leq 0.001$.

Figure 5. Validation of [^{68}Ga]Ga-AJ206 specificity for CD38 in disseminated disease models. A) IVIS-bioluminescence image of luciferase expressing MM1S disseminated tumor model (i.v) showing luciferase expression in lower limbs **B)** In vivo uptake of [^{68}Ga]Ga-AJ206 in lungs and bones **C)** Flow cytometry analysis of CD38 expression in lungs harvested from of MM1s-Luc cells injected mice. Lungs from PBS treated mice were used as controls (Top). IHC staining of bones to validate CD38 expression (bottom). **D)** In vivo and ex vivo [^{68}Ga]Ga-AJ206-PET images of lower limbs of MOLP8 injected (i.v) animals. **E)** IHC images of MOLP8 bone marrow tumor and PBS treated animals confirming CD38 expression **F)** Flow cytometry analysis of CD38 expression in cells extracted from bone marrows of PBS, MM1S-Luc and MOLP8 cell injected mice. **G)** Quantification of PET signals in the bone marrow of PBS, MM1S and MOLP8 injected animals **H)** Tumor/muscle ratios of PET measures in the bone marrows of PBS, MM1S and MOLP8 injected animals; data in figure G and H are shown as box and whisker plots showing all data points (n=7 in PBS, n=5 in MM1S and n=8 in MOLP8). Ordinary one-way ANOVA using multiple comparison test. ** $p \leq 0.01$; ****, $p \leq 0.0001$.

REFERENCES CITED.

1. Raab MS, Podar K, Breitkreutz I, Richardson PG, Anderson KC. Multiple myeloma. *Lancet* 2009;**374**(9686):324-39 doi 10.1016/S0140-6736(09)60221-X.
2. McCarthy PL, Holstein SA, Petrucci MT, Richardson PG, Hulin C, Tosi P*, et al.* Lenalidomide Maintenance After Autologous Stem-Cell Transplantation in Newly Diagnosed Multiple Myeloma: A Meta-Analysis. *J Clin Oncol* 2017;**35**(29):3279-89 doi 10.1200/JCO.2017.72.6679.
3. Kazandjian D, Landgren O. Delaying the use of high-dose melphalan with stem cell rescue in multiple myeloma is ready for prime time. *Clin Adv Hematol Oncol* 2019;**17**(10):559-68.
4. Rajkumar SV. Updated Diagnostic Criteria and Staging System for Multiple Myeloma. *Am Soc Clin Oncol Educ Book* 2016;**35**:e418-23 doi 10.1200/EDBK_159009.
5. Cowan AJ, Green DJ, Kwok M, Lee S, Coffey DG, Holmberg LA*, et al.* Diagnosis and Management of Multiple Myeloma: A Review. *Jama* 2022;**327**(5):464-77 doi 10.1001/jama.2022.0003.
6. Charalampous C, Goel U, Broski SM, Dingli D, Kapoor P, Gertz MA*, et al.* Utility of PET/CT in assessing early treatment response in patients with newly diagnosed multiple myeloma. *Blood Adv* 2022;**6**(9):2763-72 doi 10.1182/bloodadvances.2022007052.
7. Lu YY, Chen JH, Lin WY, Liang JA, Wang HY, Tsai SC*, et al.* FDG PET or PET/CT for detecting intramedullary and extramedullary lesions in multiple Myeloma: a systematic review and meta-analysis. *Clin Nucl Med* 2012;**37**(9):833-7 doi 10.1097/RLU.0b013e31825b2071.
8. Mesguich C, Fardanesh R, Tanenbaum L, Chari A, Jagannath S, Kostakoglu L. State of the art imaging of multiple myeloma: comparative review of FDG PET/CT imaging in various clinical settings. *Eur J Radiol* 2014;**83**(12):2203-23 doi 10.1016/j.ejrad.2014.09.012.
9. Caserta E, Chea J, Minnix M, Poku EK, Viola D, Vonderfecht S*, et al.* Copper 64-labeled daratumumab as a PET/CT imaging tracer for multiple myeloma. *Blood* 2018;**131**(7):741-5 doi 10.1182/blood-2017-09-807263.
10. Ghai A, Maji D, Cho N, Chanswangphuwana C, Rettig M, Shen D*, et al.* Preclinical Development of CD38-Targeted [(89)Zr]Zr-DFO-Daratumumab for Imaging Multiple Myeloma. *J Nucl Med* 2018;**59**(2):216-22 doi 10.2967/jnumed.117.196063.
11. Kang L, Jiang D, England CG, Barnhart TE, Yu B, Rosenkrans ZT*, et al.* ImmunoPET imaging of CD38 in murine lymphoma models using (89)Zr-labeled daratumumab. *Eur J Nucl Med Mol Imaging* 2018;**45**(8):1372-81 doi 10.1007/s00259-018-3941-3.
12. Kang L, Li C, Rosenkrans ZT, Huo N, Chen Z, Ehlerding EB*, et al.* CD38-Targeted Theranostics of Lymphoma with (89)Zr/(177)Lu-Labeled Daratumumab. *Adv Sci (Weinh)* 2021;**8**(10):2001879 doi 10.1002/advs.202001879.
13. Kang L, Li C, Yang Q, Sutherlin L, Wang L, Chen Z*, et al.* (64)Cu-labeled daratumumab F(ab')(2) fragment enables early visualization of CD38-positive lymphoma. *Eur J Nucl Med Mol Imaging* 2022;**49**(5):1470-81 doi 10.1007/s00259-021-05593-9.
14. Li S, England CG, Ehlerding EB, Kutyreff CJ, Engle JW, Jiang D*, et al.* ImmunoPET imaging of CD38 expression in hepatocellular carcinoma using (64)Cu-labeled daratumumab. *Am J Transl Res* 2019;**11**(9):6007-15.
15. Ulaner GA, Sobol NB, O'Donoghue JA, Kirov AS, Riedl CC, Min R*, et al.* CD38-targeted Immuno-PET of Multiple Myeloma: From Xenograft Models to First-in-Human Imaging. *Radiology* 2020;**295**(3):606-15 doi 10.1148/radiol.2020192621.
16. Cho N, Ko S, Shokeen M. Preclinical Development of Near-Infrared-Labeled CD38-Targeted Daratumumab for Optical Imaging of CD38 in Multiple Myeloma. *Mol Imaging Biol* 2021;**23**(2):186-95 doi 10.1007/s11307-020-01542-4.
17. Cho N, Ko S, Shokeen M. Tissue biodistribution and tumor targeting of near-infrared labelled anti-CD38 antibody-drug conjugate in preclinical multiple myeloma. *Oncotarget* 2021;**12**(20):2039-50 doi 10.18632/oncotarget.28074.
18. Wang C, Chen Y, Hou YN, Liu Q, Zhang D, Zhao H*, et al.* ImmunoPET imaging of multiple myeloma with [(68)Ga]Ga-NOTA-Nb1053. *Eur J Nucl Med Mol Imaging* 2021;**48**(9):2749-60 doi 10.1007/s00259-021-05218-1.
19. Deaglio S, Mehta K, Malavasi F. Human CD38: a (r)evolutionary story of enzymes and receptors. *Leuk Res* 2001;**25**(1):1-12 doi 10.1016/s0145-2126(00)00093-x.

20. van de Donk N, Usmani SZ. CD38 Antibodies in Multiple Myeloma: Mechanisms of Action and Modes of Resistance. *Front Immunol* 2018;**9**:2134 doi 10.3389/fimmu.2018.02134.
21. van de Donk N, Richardson PG, Malavasi F. CD38 antibodies in multiple myeloma: back to the future. *Blood* 2018;**131**(1):13-29 doi 10.1182/blood-2017-06-740944.
22. Teufel D, Mudd G, Pavan S; BICYCLETX LIMITED [GB]/[GB], assignee. Peptide ligands for binding to CD38, WO/2019/243353. GB26.12.2019.
23. Ebenhan T, Chadwick N, Sathekge MM, Govender P, Govender T, Kruger HG*, et al.* Peptide synthesis, characterization and (6)(8)Ga-radiolabeling of NOTA-conjugated ubiquicidin fragments for prospective infection imaging with PET/CT. *Nucl Med Biol* 2014;**41**(5):390-400 doi 10.1016/j.nucmedbio.2014.02.001.
24. Ogiya D, Liu J, Ohguchi H, Kurata K, Samur MK, Tai YT*, et al.* The JAK-STAT pathway regulates CD38 on myeloma cells in the bone marrow microenvironment: therapeutic implications. *Blood* 2020;**136**(20):2334-45 doi 10.1182/blood.2019004332.
25. Martin TG, Corzo K, Chiron M, Velde HV, Abbadessa G, Campana F*, et al.* Therapeutic Opportunities with Pharmacological Inhibition of CD38 with Isatuximab. *Cells* 2019;**8**(12) doi 10.3390/cells8121522.
26. Zhu C, Song Z, Wang A, Srinivasan S, Yang G, Greco R*, et al.* Isatuximab Acts Through Fc-Dependent, Independent, and Direct Pathways to Kill Multiple Myeloma Cells. *Front Immunol* 2020;**11**:1771 doi 10.3389/fimmu.2020.01771.
27. Nijhof IS, Groen RW, Lokhorst HM, van Kessel B, Bloem AC, van Velzen J*, et al.* Upregulation of CD38 expression on multiple myeloma cells by all-trans retinoic acid improves the efficacy of daratumumab. *Leukemia* 2015;**29**(10):2039-49 doi 10.1038/leu.2015.123.
28. Nijhof IS, Casneuf T, van Velzen J, van Kessel B, Axel AE, Syed K*, et al.* CD38 expression and complement inhibitors affect response and resistance to daratumumab therapy in myeloma. *Blood* 2016;**128**(7):959-70 doi 10.1182/blood-2016-03-703439.
29. Lokhorst HM, Plesner T, Laubach JP, Nahi H, Gimsing P, Hansson M*, et al.* Targeting CD38 with Daratumumab Monotherapy in Multiple Myeloma. *N Engl J Med* 2015;**373**(13):1207-19 doi 10.1056/NEJMoa1506348.
30. Lonial S, Weiss BM, Usmani SZ, Singhal S, Chari A, Bahlis NJ*, et al.* Daratumumab monotherapy in patients with treatment-refractory multiple myeloma (SIRIUS): an open-label, randomised, phase 2 trial. *Lancet* 2016;**387**(10027):1551-60 doi 10.1016/S0140-6736(15)01120-4.
31. Usmani SZ, Weiss BM, Plesner T, Bahlis NJ, Belch A, Lonial S*, et al.* Clinical efficacy of daratumumab monotherapy in patients with heavily pretreated relapsed or refractory multiple myeloma. *Blood* 2016;**128**(1):37-44 doi 10.1182/blood-2016-03-705210.
32. Krishnan A, Adhikarla V, Poku EK, Palmer J, Chaudhry A, Biglang-Awa VE*, et al.* Identifying CD38+ cells in patients with multiple myeloma: first-in-human imaging using copper-64-labeled daratumumab. *Blood Adv* 2020;**4**(20):5194-202 doi 10.1182/bloodadvances.2020002603.
33. Kumar D, Lisok A, Dahmane E, McCoy M, Shelake S, Chatterjee S*, et al.* Peptide-based PET quantifies target engagement of PD-L1 therapeutics. *J Clin Invest* 2019;**129**(2):616-30 doi 10.1172/JCI122216.
34. Kumar D, Mishra A, Lisok A, Kureshi R, Shelake S, Plyku D*, et al.* Pharmacodynamic measures within tumors expose differential activity of PD(L)-1 antibody therapeutics. *Proc Natl Acad Sci U S A* 2021;**118**(37) doi 10.1073/pnas.2107982118.
35. Mishra A, Kumar D, Gupta K, Lofland G, Sharma AK, Banka DS*, et al.* Gallium-68-labeled Peptide PET Quantifies Tumor Exposure of PD-L1 Therapeutics. *Clin Cancer Res* 2022 doi 10.1158/1078-0432.CCR-22-1931.
36. Frerichs KA, Minnema MC, Levin MD, Broijl A, Bos GMJ, Kersten MJ*, et al.* Efficacy and safety of daratumumab combined with all-trans retinoic acid in relapsed/refractory multiple myeloma. *Blood Adv* 2021;**5**(23):5128-39 doi 10.1182/bloodadvances.2021005220.